J Mater Sci: Mater Med (2010) 21:1531–1542
DOI 10.1007/s10856-010-4031-7

Crystallographically engineered, hydrothermally crystallized hydroxyapatite films: an in vitro study of bioactivity

Daniel J. Haders · Christian C. Kazanecki · David T. Denhardt · Richard E. Riman

Received: 1 August 2009 / Accepted: 15 February 2010 / Published online: 16 March 2010

Abstract The aim of this study was to evaluate the bioactivity of hydroxyapatite films composed of hexagonal single crystals that display $\{10\bar{1}0\}$ and {0001} crystallographic faces. The effect of engineered [0001] crystallographic orientation was investigated in parallel. Films were deposited by triethyl phosphate/ethylenediamine-tetraacetic acid doubly regulated hydrothermal crystallization on Ti6Al4V substrates (10, 14, 24 h). Bioactivity was investigated by analysis of MC3T3-E1 pre-osteoblast spreading using scanning electron microscopy and quantitative analysis of cell metabolic activity (Alamar Blue^{TM}) (0–28 days). Scanning electron microscopy and X-ray diffraction were used to evaluate the ability of films to support the differentiation of MC3T3-E1 pre-osteoblasts into matrix-secreting, mineralizing osteoblasts. Results demonstrated that all films enabled MC3T3-E1 cells to spread, grow, and differentiate into matrix-secreting osteoblasts, which deposited biomineral that could not be removed after extraction of organic material. Differences in [0001] HA crystallographic orientation were not, however, found to significantly affect bioactivity. Based on these results, it is concluded that these hydrothermal hydroxyapatite films are non-toxic, bioactive, osteoconductive, and biomineral bonding. The lack of a relationship between reported hydroxyapatite crystallographic face specific protein adsorption and bulk HA bioactivity are discussed in terms of crystallographic texture, surface roughness, assay robustness, and competitive protein adsorption.

Abbreviations

HA	Hydroxyapatite
PS-HA	Plasma sprayed hydroxyapatite
EDTA	Ethylenediamine-tetraacetic acid, $C_{10}H_{16}N_2O_8$
TEP	Triethyl phosphate, $C_6H_{15}O_4P$
Ca-P	Calcium-phosphate
XRD	X-ray diffraction
FESEM	Field emission scanning electron microscopy
TCP	Tissue culture plastic
PDF	Powder diffraction file
Ti6Al4V	Alloyed titanium with 6 wt% aluminum and 4 wt% vanadium
(*hkil*)	Hexagonal crystallographic plane Miller indices
{*hkil*}	Equivalent hexagonal crystallographic plane Miller indices
[*uvtw*]	Hexagonal crystallographic direction

1 Introduction

Commercial hydroxyapatite (HA) films are most often applied to metallic substrates for orthopedic applications using the plasma spray method (PS-HA), which is a high temperature process that sprays molten hydroxyapatite particles onto the implant surface at high pressures [1–3]. Since the introduction of PS-HA coatings in the 1980s [3], however, concerns have been raised about the consequences of PS-HA's low crystallinity, lack of phase purity,

D. J. Haders · R. E. Riman (✉)
Department of Material Science and Engineering, Rutgers, The State University of New Jersey, Piscataway, NJ, USA
e-mail: riman@rci.rutgers.edu

D. J. Haders · R. E. Riman
Department of Biomedical Engineering, Rutgers, The State University of New Jersey, Piscataway, NJ, USA

C. C. Kazanecki · D. T. Denhardt
Department of Cell Biology and Neuroscience, Rutgers, The State University of New Jersey, Piscataway, NJ, USA

passivation properties, and difficulty in coating substrates with complex geometry (line-of-sight-process) [1, 3–9]. Critically, PS-HA films applied to the clinically relevant Ti6Al4V alloy (alloyed titanium with 6 wt% aluminum and 4 wt% vanadium) lack a Ti–HA chemical intermediate bonding layer such as $CaTiO_3$, and rely on mechanical interlock rather than chemical bonding to adhere the film to the substrate [6–8]. As a result, in vivo coating delamination has been reported due to the greater interfacial strength between HA and bone, than HA and titanium [10–14]. HA films deposited by other techniques including sol–gel, pulsed laser deposition, magnetron sputtering, ion-beam deposition, and biomimetic crystallization share all or some of PS-HA's limitations [15–20]. Consequently, there is a need to develop inexpensive reproducible next generation HA film deposition techniques, which deposit chemically bonded, high crystallinity, phase-pure, passivating, conformal HA films on clinically used substrates such as Ti6Al4V.

We have previously reported on the use of triethyl phosphate (TEP)/ethylenediamine-tetraacetic acid (EDTA) doubly regulated hydrothermal crystallization to deposit HA films on metallic substrates [21, 22]. Results demonstrated that highly crystalline, phase-pure, passivating HA films were formed on all examined substrates. The utilization of the delayed-release phosphate source, TEP, enabled the deposition of $CaTiO_3$ and then HA in a single, phase-sequenced process on Ti substrates, the first process of its kind reported in the hydrothermal HA literature. The process chemically bonded HA to Ti, which enabled a high film adhesion value to be obtained (5, ASTM D3359). It was also demonstrated that films were composed of hexagonal single crystals of HA, which display the $\{10\bar{1}0\}$ ($\{hkil\}$—equivalent hexagonal crystallographic plane Miller indices) crystallographic face on the six equivalent hexagonal faces and the $\{0001\}$ face on the cap of the hexagonal rod. Importantly, molecular modeling and in vitro studies have shown that acidic bone proteins and other proteins found to bind HA with high affinity, bind to the $\{10\bar{1}0\}$ face [23, 24]. Thus, it is hypothesized that the films reported here will demonstrate robust bioactivity due to the functionalization of the film surface with highly bioactive HA crystallographic faces, which together with previously reported material properties, including film-substrate chemical bonding, will make these films potential candidates for use on clinical Ti6Al4V orthopedic implants.

Previous work also demonstrated that the [0001] ([*uvtw*]—hexagonal crystallographic direction), *c*-axis, crystallographic orientation (texture) of hexagonal single crystals of HA could be engineered through control of synthesis time [22]. By taking advantage of the ability to control crystal surfaces (faces) and crystallographic texture this film deposition process may enable a novel route to further functionalize the film surface with highly bioactive crystallographic faces. More specifically, engineering the orientation of hexagonal HA crystals may, together with aspect ratio and crystal spacing, enable the ratio of $\{10\bar{1}0\}/\{0001\}$ faces presented to the extracellular fluid to be altered, allowing modulation of protein adhesion, bioactivity, and potentially properties such as implant integration and healing time. For example, crystals that compose the 10 h film have an aspect ratio of approximately 1, no spacing between the crystals, and a nominally random [0001] orientation indicating that there is likely a nominally equal representation of $\{10\bar{1}0\}$ and $\{0001\}$ planes on the film surface. Crystals that compose the 24 h film have a larger aspect ratio, spacing between crystals, and a large volume fraction of crystals with their [0001] direction near $2\theta = 0°$ potentially creating a large $\{10\bar{1}0\}/\{0001\}$ ratio. In addition to the crystal face specific protein adsorption data cited above, others have demonstrated that self-directed HA protein adsorption and matrix formation from serum increases cell attachment and spreading as compared to HA surfaces functionalized with integrin binding (RGD) and proteoglycan binding peptides [25], indicating that HA contains all the surface functionalization cues necessary for efficient protein adsorption, initial matrix formation, and cell attachment within its own crystal structure. Thus, it is hypothesized that these surface functionalization cues may be accentuated by engineering both crystal morphology and crystallographic orientation.

Although not the focus of this paper, it is recognized that surface roughness is also an important cell biology variable for tailoring bioactivity. For example, surface roughness has been reported to affect the spreading, proliferation, and differentiation (alkaline phosphatase (ALP) activity, type I collagen production, and *Runx 2* gene expression) of pre-osteoblast cells on titanium substrates [26, 27]. Previous studies from our laboratory demonstrate obvious differences in the surface roughness profiles of HA films with differing degrees of [0001] crystallographic orientation [22]. Thus, it is critical that any substrate-dependent changes in MC3T3-E1 behavior be evaluated in terms of both [0001] crystallographic orientation and substrate surface roughness.

This study examines the effect of crystal faces and crystal orientation on HA film bioactivity. Bioactivity is evaluated by observation of cell spreading and quantitative analysis of total cell metabolic activity on hydrothermally crystallized HA films deposited for 10, 14, and 24 h with differing degrees of [0001] crystallographic orientation. The ability of these adherent films to support the differentiation of pre-osteoblasts into matrix secreting, mineralizing osteoblasts is then evaluated.

2 Materials and methods

2.1 HA film synthesis and Ti6Al4V substrate preparation

Ti6Al4V was chosen as the metallic substrate for this study due to both its clinical use in load-bearing orthopedic applications, and results for HA films previously deposited by the method reported here, on this substrate [21, 22]. Previous results from our laboratory demonstrate the crystallization of adhesive (5, ASTM D3359) chemically bonded films composed of hexagonal single crystals of HA that display $\{10\bar{1}0\}$ and $\{0001\}$ HA crystallographic faces. Results have also demonstrated that the [0001] crystallographic orientation of HA films may be engineered through control of synthesis time. At 10 h, the [0001] orientation of crystals is nominally random, at 24 h the volume fraction of crystals with their [0001] direction parallel to the sample surface is several multiples greater than expected for a randomly oriented sample, and at 14 h an intermediate [0001] texture is obtained. Thus, here, Ti6Al4V substrates (McMaster Carr, Dayton, NJ) were treated hydrothermally for 10, 14, and 24 h using the previously reported hydrothermal crystallization process and used to investigate the bioactivity of chemically bonded HA films composed of hexagonal single crystals with engineered [0001] crystallographic texture.

Ti6Al4V was utilized as an internal standard for bioactivity testing due to its clinical use in load-bearing orthopedic applications. Both polished and roughened Ti6Al4V substrates were used so that differences in bioactivity could be interpreted in terms of surface roughness, irrespective of crystallographic orientation. Polished Ti6Al4V samples were the same as those used for HA film deposition. Roughened Ti6Al4V alloy substrates were formed by grit blasting polished Ti6Al4V samples using 35–100 Al_2O_3 media (McMaster Carr). Grit was removed by cleaning in an ultrasonic bath (FS30, Fisher Scientific, Hampton, NH). All Ti6Al4V samples were then cleaned with detergent (Alconox, White Plains, NY), ethyl alcohol (Pharmco-AAPER, Brookfield, CT), and distilled water.

2.2 Film/substrate characterization

The surface roughness, R_a, of 10, 14, and 24 h HA films was measured by profilometry (scan length 500 μm, Dektak 3030, Veeco, Woodbury, NY). The average surface roughness of six measurements for each film type, and the standard deviation of the means were calculated. Polished Ti6Al4V and roughened Ti6Al4V substrates were characterized by profilometry in a previous study [21]. To determine if differences in surface roughness were statistically significant ($P < 0.05$) a One Way ANOVA was calculated (Excel 2000, Microsoft, Redmond, WA) followed by a Tukey's Honest Significant Difference (HSD) post-test [28].

2.3 In vitro cell culture work

MC3T3-E1 subclone 4, mouse calvaria-derived, pre-osteoblast cells [29] were used to study the biocompatibility of crystallographically tuned HA films synthesized for 10, 14, and 24 h on Ti6Al4V substrates; in addition to polished and roughened Ti6Al4V substrates, which were used as internal standards. Cells were cultured at 37°C and 5% CO_2 (Forma Scientific, Marietta, OH) in complete cell growth medium—α-Minimum Essential Medium (α-MEM) (Invitrogen Corp, Carlsbad, CA), 10% Fetal Bovine Serum (FBS) (Hyclone, Logan UT), 50 units/ml penicillin (Invitrogen Corp), 50 μg/ml streptomycin (Invitrogen Corp), and 1 mM glutamine (Invitrogen Corp)—prior to seeding onto samples. Specimens were sterilized by autoclaving for 20 min with a 10 min dry cycle (Consolidated Stills and Sterilizers, Boston, MA), and placed in individual wells of a six-well tissue culture plate (Falcon, Becton–Dickinson and Company, Franklin Lakes, NJ) under sterile conditions for all studies. Cells were then seeded onto specimens at the densities noted below in complete cell growth medium and incubated. Tissue culture plastic (TCP) was used as a control for all studies. For some experiments, cells were switched to complete induction medium—α-MEM (Invitrogen Corp), 10% FBS (Hyclone), 50 units/ml penicillin (Invitrogen Corp), 50 μg/ml streptomycin (Invitrogen Corp), 1 mM glutamine (Invitrogen Corp), 50 μg/ml ascorbic acid (Sigma–Aldrich, St. Louis, MO), and 10 mM β-glycerol-phosphate (Sigma–Aldrich)—at the indicated times.

2.3.1 Cell spreading

The general bioactivity of substrates was evaluated, in terms of cell spreading, by seeding MC3T3-E1 subclone 4 passage 17 cells onto TCP, polished Ti6Al4V, roughened Ti6Al4V, and HA films synthesized on polished Ti6Al4V for 10, 14, and 24 h at a density of $1 \cdot 10^4$ cells/cm^2 in complete cell growth medium, and allowing them to attach and spread for 3 days. Cells were then fixed by incubating in cold 2% glutaraldehyde (Fisher Scientific) in phosphate-buffered saline (PBS) for 2 h, washed twice in PBS (15 min each), rinsed twice with distilled water (10 min each), and dehydrated by incubating in 50, 70, 80, 95, 100, and 100 vol.% ethanol (Pharmco-AAPER) for 15 min each. Samples were then critical point dried (CPD 020, OC Oerlikon Balzers AG, Balzers, Liechtenstein), sputter coated with a conducting ~25 nm Au/Pd film (SCD 004, OC Oerlikon Balzers AG), and observed by field emission scanning electron microscopy (FESEM, Model DSM 962 Gemini, Carl Zeiss, Oberkochen, Germany).

2.3.2 Cell metabolic activity: Alamar Blue™ assay

The ability of substrates to support osteoblast cell growth, in terms of total cell metabolic activity, was evaluated by seeding MC3T3-E1 subclone 4 passage 15 cells onto TCP, polished Ti6Al4V, roughened Ti6Al4V, and HA films synthesized on polished Ti6Al4V for 10, 14, and 24 h at a density of $1 \cdot 10^4$ cells/cm^2 in complete cell growth medium, and incubating. All samples were studied in triplicate. Cells were allowed to attach for 1 day after which polished Ti6Al4V, roughened Ti6Al4V, and 10, 14, and 24 h HA film samples were moved to wells in new six-well plates containing fresh complete cell growth medium under sterile conditions. This was done to eliminate cells from assay measurements that were attached to the tissue culture plastic rather than the samples. For consistency, complete cell growth medium was changed on TCP wells at this time. Triplicate blank wells containing only complete growth medium were also added at this time. This point was considered 0 days.

Alamar Blue™ (BioSource International, Camarillo, CA) is a dye that is taken up by cells and reduced from a non-fluorescent state to a fluorescent state by metabolic intermediates. At the following intervals, 0, 1, 3, 5, 8, 13, 15, 17, 20, 24, and 28 days, it was added to each culture well to a final concentration of 10%. After 2 h, 3–250 µl replicate aliquots were taken from each well and placed in a 96-well plate. Fluorescence was measured by exiting at 530 nm and measuring emission at 590 nm using a fluorometer (FluoroCount, Packard Instrument Co., Meriden CT). After each measurement, or every 2–3 days, the cell growth medium was removed, samples/wells were rinsed in PBS and fresh complete induction medium was added.

Data were expressed as a fraction of cell activity on the TCP control using the following equation:

$$\alpha = \frac{S_i - B_i}{C_i - B_i} \quad (1)$$

where S_i is sample fluorescence intensity, C_i is TCP/control fluorescence intensity, B_i is blank/background fluorescence intensity, and α is cell activity as a fraction of control. The average cell activity for each sample type and the standard deviation of the means were calculated. To determine if differences in cell activity between sample groups at each time point were statistically significant ($P < 0.05$) a one way ANOVA was calculated (Excel 2000, Microsoft) followed by a Tukey's Honest Significant Difference (HSD) post-test [28].

2.3.3 Cell differentiation: extracellular matrix formation

The ability of substrates to support osteoblast cell differentiation in terms of extracellular matrix formation was evaluated by seeding MC3T3-E1 subclone 4 passage 15 cells onto TCP, polished Ti6Al4V, roughened Ti6Al4V, and HA films synthesized on polished Ti6Al4V for 10, 14, and 24 h at a density of $1 \cdot 10^4$ cells/cm^2 in complete cell growth medium, and incubating. After 1 day, the cell growth medium was changed to complete induction medium. Therefore, the medium was then changed every 2–3 days. After 105 days (15 weeks) samples were fixed, dehydrated, critical point dried, and sputter coated, as above, and then observed by FESEM (DSM 982 Gemini, Carl Zeiss).

2.3.4 Cell differentiation: mineralization

The ability of substrates to support osteoblast cell differentiation, in terms of biomineralization, was evaluated by seeding MC3T3-E1 subclone 4 passage 15 cells onto TCP, polished Ti6Al4V, roughened Ti6Al4V, and HA films synthesized on polished Ti6Al4V for 10, 14, and 24 h at a density of $1 \cdot 10^4$ cells/cm^2 in complete cell growth medium and incubating. After 1 day, the medium was changed to complete induction medium. Thereafter, the medium was changed every 2–3 days. After 98 days (14 weeks) samples were removed from the incubator and washed twice in PBS. Organic cell layers were then extracted by adding 6.15 vol.% sodium hypochlorite (Ultra Clorox Bleach, The Clorox Company, Oakland, C.A.) to each sample well, and placing the culture plate in an 85°C water bath for 2 h as previously described [30]. The liquid/mineral suspension was removed from each well, and placed in a 15 ml conical tube. Each well/sample was then rinsed twice in distilled water, and this was also added to the corresponding 15 ml conical tube. Mineral suspensions were then centrifuged for 3 min at $210 \times g$ in a clinical centrifuge (International Equipment Company, Nashville, TN). The supernatant was removed, 10 ml of fresh distilled water was added, and samples were entrifuged again. This process was repeated three times. All supernatant except ~250 µl was then removed. The remaining solution was then pipetted to re-create a biomineral suspension. The suspension was removed and added drop-wise onto a glass slide, creating as small of a footprint as possible. The glass slides were then dried at 70°C for 1–2 h. The resulting powder biomineral samples were then examined by X-ray diffraction (XRD) (step size = 0.02°, 4 step/s, 45 kV, 40 mA, Ni-filtered CuK_α radiation, parallel beam optics, Philips Hi-Resolution X'PERT X-Ray Diffractometer, PANalytical B.V., Almelo, Netherlands) and FESEM (DSM 982 Gemini, Carl Zeiss). Experimental XRD patterns were matched to patterns in the Powder Diffraction File (PDF, ICDD, Newtown Square, PA) database using Jade 8.0 software (MDI, Livermore, CA). The substrates (polished Ti6Al4V, roughened Ti6Al4V, and 10, 14, and 24 h HA films) were also dried at 70°C for 1–2 h and then examined by FESEM (DSM 982 Gemini, Carl Zeiss).

3 Results

3.1 Substrate characterization

Polished Ti6Al4V (P-Ti6Al4V), roughened Ti6Al4V (R-Ti6Al4V), and HA films hydrothermally synthesized on polished Ti6Al4V for 10, 14, and 24 h have been extensively characterized previously [21, 22]. Surface roughness, R_a, results for 10, 14, and 24 h HA samples obtained in this study are reported in Table 1 along with previously reported values for P-Ti6Al4V and R-Ti6Al4V. Results demonstrate an increase in surface roughness with synthesis time, and average values that fall between that of P-Ti6Al4V ($R_a = 414$ nm) and R-Ti6Al4V ($R_a = 3{,}569$ nm). Statistical analysis by ANOVA and Tukey HSD demonstrate that differences in surface roughness values between samples were statistically significant ($P < 0.05$). Surface roughness is an important cell biology variable and has been reported to affect the spreading, proliferation, and differentiation (alkaline phosphatase (ALP) activity, type I collagen production, and *Runx 2* gene expression) of pre-osteoblast cells on titanium substrates [26, 27]. Based on this information, it is concluded that differences in MC3T3-E1 behavior are possible in this study due to differences in substrate surface roughness.

Table 1 Substrate surface roughness (*Ra*)

Substrate	Roughness, Ra (nm)
R-Ti6Al4V	3569 +/- 1014*
24 h	2975 +/- 600
14 h	2025 +/- 445
10 h	1096 +/- 87
P-Ti6Al4V	414 +/- 81*

* Data presented previously in Haders et al. [21]. *Bars* indicate samples with statistically significant differences in surface roughness

3.2 Cell spreading

General substrate bioactivity was evaluated by observation of cell spreading on P-Ti6Al4V, R-Ti6Al4V, and 10, 14, and 24 h HA films (Fig. 1). The cell spreading assay is a qualitative assay that evaluates the general bioactivity of a surface. Cells in contact with toxic surfaces minimize their surface area that is in contact with those surfaces, while cells in contact with bioactive surfaces maximize their surface area. Figure 1 displays MC3T3-E1 subclone 4 pre-osteoblast cells on substrates after 3 days in culture. In general, it is observed that cells are attached and spread on all substrates, such that they are extended more than 40 μm in their longest direction. This result is comparable to MC3T3-E1 cell spreading on HA films reported elsewhere [31]. From these results it is concluded both that all substrates are non-toxic and biocompatible and that the HA films reported here display results similar to those reported in the HA literature.

For Ti6Al4V substrates, a difference in average surface roughness of ~3 μm is observed to significantly affect MC3T3-E1 cell spreading. Cell spreading on P-Ti6Al4V ($R_a = 414$ nm) is two-dimensional. Spreading is directed along and within the polishing grooves on the substrate. This observation agrees with reports of contact guidance reported previously for MC3T3-E1 cells on grooved Ti6Al4V substrates [32]. On the other hand, cell spreading on R-Ti6Al4V ($R_a = 3{,}569$ nm) is observed to be three-dimensional. Spreading occurs over and around surface features of different heights with cell filopodia and cell bodies that bridge gaps from one surface feature to the next. It is also observed that the aspect ratio of cells is affected by surface roughness. Cells on polished Ti6Al4V

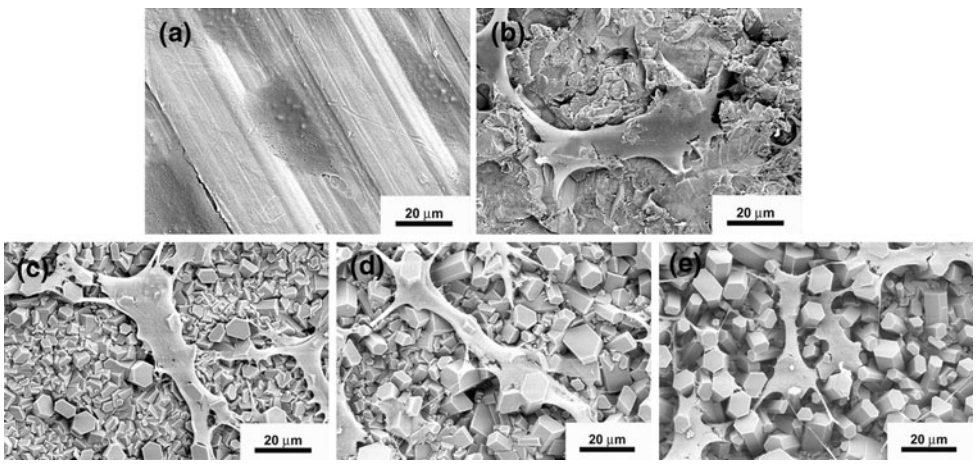

Fig. 1 Scanning electron micrographs of MC3T3-E1 subclone 4 p.17 pre-osteoblast cell spreading on substrates after 3 days in cell culture: **a** P-Ti6Al4V, **b** R-Ti6Al4V, **c** HA 10 h, **d** HA 14 h, **e** HA 24 h

fill the entire width of the grooves and have aspect ratios of ~1–2 as compared to cells on R-Ti6Al4V, which have aspect ratios of ~5. Differences in neither average surface roughness (~1.9 μm) nor [0001] crystallographic orientation were found to have a significant affect on cell spreading on HA films, however. Cells on all HA samples demonstrated spreading patterns similar to that seen on R-Ti6Al4V. Interestingly, 10, 14, and 24 h samples like the R-Ti6Al4V sample have micron scale surface roughness, as compared to the nanometer scale surface roughness of P-Ti6Al4V sample. From this result, it may be concluded that changes in substrate surface roughness from the nanometer scale (P-Ti6Al4V) to the micron scale (R-Ti6Al4V, 10, 14, 24 h) affects MC3T3-E1 cell spreading patterns in the same general manner on these substrates, regardless of substrate chemistry or [0001] crystallographic orientation. Differences in micron scale roughness between HA samples or between HA and the R-Ti6Al4V sample do not lead to a measurable effect on cell spreading.

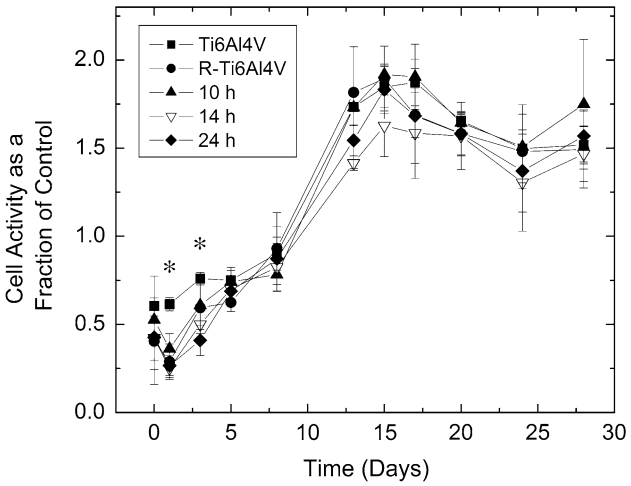

Fig. 2 Total cell metabolic activity of MC3T3-E1 subclone 4 p.15 osteoblast-like cells on various substrates as a fraction of TCP control from 0 to 28 days measured using the Alamar Blue™ biochemical assay. * Indicates statistically significant ($P < 0.05$) difference in measured cell activity between substrate types at a specific time point

3.3 Metabolic activity

The ability of P-Ti6Al4V, R-Ti6Al4V, and 10, 14, and 24 h HA films to support the growth of cell cultures was measured in terms of total metabolic activity using the Alamar Blue™ assay. Figure 2 displays the metabolic activity profiles of MC3T3-E1 subclone 4 cell cultures from 0 to 28 days as a fraction of TCP controls. All substrates demonstrate a significant, multi-fold increase in metabolic activity from day 0 to their peak at day 15 or day 17. After this time, total metabolic activity levels stagnate and decline due to the formation of confluent cell layers. In reference to the HA literature, cell activity as a fraction of control at day 0, 1, and 3 on all HA substrates is comparable to the best performing HA films reported by Ball et al. [33] at day 2, using the same assay. The increase in non-normalized cell activity is 3–4 fold from day 3 to day 13 (data not shown), as compared to a single fold increase in the same parameter for the best performing HA films reported by Thian et al. [34] between day 3 and day 14, using the same assay. Thus, it is concluded both that all substrates support the growth of MC3T3-E1 culture total metabolic activity, and consequently cell number, and that the HA films reported here display results comparable to those reported in the HA literature.

For Ti6Al4V substrates, a difference in average surface roughness of ~3 μm is observed to significantly ($P < 0.05$) affect total metabolic activity at day 1. Differences in metabolic activity are statistically insignificant at all other time points. These results are not unexpected. Reduced rates of cell proliferation and reduced cell number have been reported previously and attributed to increasing surface roughness on Ti6Al4V substrates for MC3T3-E1 and MG63 osteoblast-like cells, respectively, at early culture time points [26, 27]. Differences in neither average surface roughness (~1.9 μm) nor [0001] crystallographic orientation were found to have a significant ($P > 0.05$) effect on MC3T3-E1 metabolic activity on HA films, however. This is unexpected at least in terms of surface roughness based upon the work of Kim et al., which demonstrated significant differences in cell proliferation between Ti surfaces with surface roughness values similar to the HA films reported here, ~1–3 μm [27]. In general, however, metabolic activity patterns on all HA samples were similar to that seen on R-Ti6Al4V. All HA films demonstrated significantly ($P < 0.05$) lower total metabolic activity levels on day 1 as compared to cells on P-Ti6Al4V. The 24-h film had significantly lower metabolic activity levels on day 3 as well. Thus, it is concluded that changes in substrate surface roughness from the nanometer scale (P-Ti6Al4V) to the micron scale (R-Ti6Al4V, 10, 14, 24 h) affect MC3T3-E1 culture total metabolic activity patterns in the same general manner on these substrates, regardless of substrate chemistry or [0001] crystallographic orientation. Differences in micron scale roughness between HA samples or between HA and the R-Ti6Al4V sample do not lead to a measurable effect on total metabolic activity.

3.4 Cell differentiation: extracellular matrix

The ability of substrates to support the differentiation of MC3T3-E1 subclone 4 pre-osteoblasts into mature, matrix-secreting osteoblasts was evaluated by culturing cells for 105 days on each substrate. Scanning electron micrographs of the surface of TCP, P-Ti6Al4V, R-Ti6Al4V, and 10, 14,

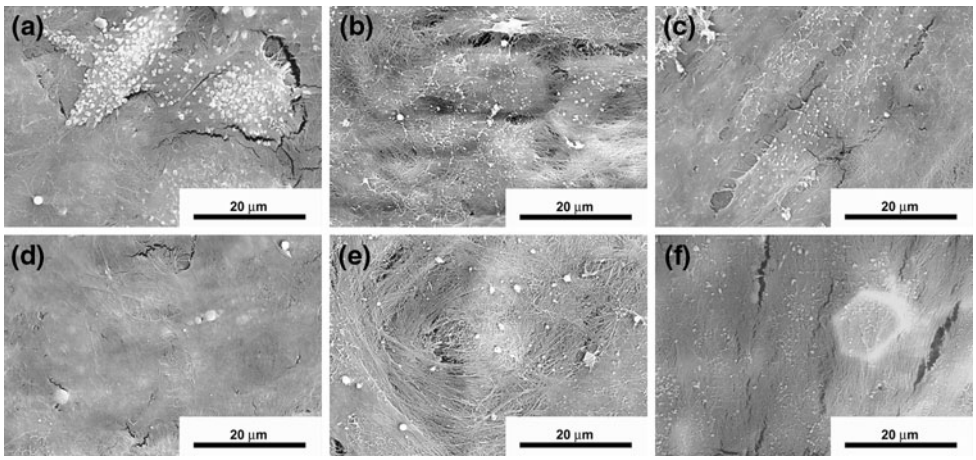

Fig. 3 Scanning electron micrographs of MC3T3-E1 subclone 4 p.15 osteoblast-like cells and their deposited extracellular matrix on various substrates after 105 days in culture: **a** TCP, **b** P-Ti6Al4V, **c** R-Ti6Al4V, **d** HA 10 h, **e** HA 14 h, **f** HA 24 h

and 24 h HA films after 105 days in culture are displayed in Fig. 3. All micrographs demonstrate the formation of an extensive extracellular matrix that completely covers and obscures the topology of the underlying substrate. The only observable substrate features are "shadows" of hexagonal HA crystals under the surface of the extracellular matrix formed on the 24 h sample. Thus, it may be concluded that all substrates support the differentiation of MC3T3-E1 subclone 4 pre-osteoblasts into mature, matrix-secreting osteoblasts. No difference in gross extracellular matrix formation was observed in terms of [0001] crystallographic orientation on HA substrates, or in terms of surface roughness on HA and Ti6Al4V substrates.

3.5 Cell differentiation: mineralization

The ability of substrates to support the differentiation of MC3T3-E1 subclone 4 pre-osteoblasts into fully differentiated, mineralizing osteoblasts was evaluated by culturing cells for 98 days on each substrate, chemically removing the cell/ECM layer (6.15 vol.% sodium hypochlorite), and pelleting the non-solubilized mineralized portion of the matrix. Figures 4 and 5 display XRD patterns and SEM micrographs of the mineralized portion of the extracellular matrix isolated from TCP, P-Ti6Al4V, and R-Ti6Al4V substrates. No measurable amount of biomineral was isolated from the cell layers extracted from HA films. All observed peaks in the XRD patterns correspond to HA diffraction peaks reported in the powder diffraction file (PDF). Patterns are similar to those reported in the literature for in vitro biomineral deposited in MC3T3-E1 and fresh rat marrow cell cultures, and rat cortical bone [30, 35]. The large background hump below $2\theta = 30°$ has been attributed to residual extracellular matrix [35]. Scanning electron micrographs of the biomineral on all substrates display a fibrous structure, which reflects the structure of the extracellular matrix that was deposited and subsequently mineralized. All the various microstructures

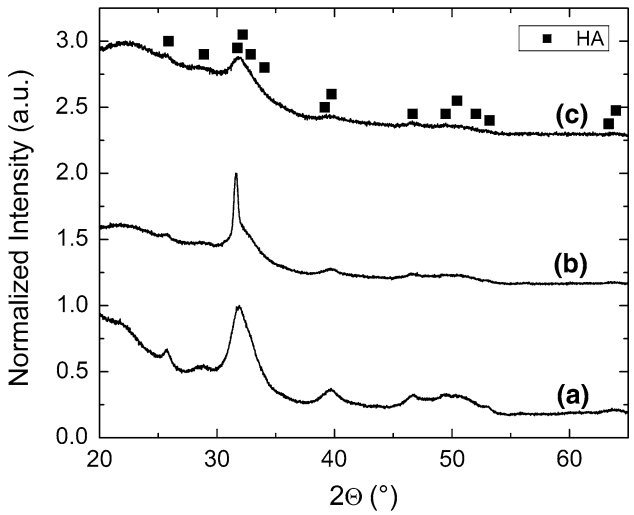

Fig. 4 X-ray diffraction patterns of biomineral harvested from various substrates seeded with MC3T3-E1 subclone 4 p.15 osteoblast-like cells after 98 days in culture: **a** TCP, **b** P-Ti6Al4V, **c** R-Ti6Al4V

observed in Fig. 5 were observed for all substrates. Thus, it may be concluded that TCP, P-Ti6Al4V, and R-Ti6Al4V substrates all support the differentiation of pre-osteoblasts cultures into fully differentiated, mineralizing osteoblasts as reported extensively elsewhere.

No mineral was isolated from cell layers extracted from HA films. Consequently, the ability of the HA films reported here to support the differentiation of MC3T3-E1 subclone 4 pre-osteoblasts into fully differentiated, mineralizing osteoblasts is unclear from the data reported above. To further evaluate differentiation the surface of each substrate was examined after chemical removal of the cell/ECM layer. SEM analysis of HA substrates revealed the presence of inorganic nodules on the surface of each HA film (Fig. 6). SEM analysis of polished and roughened Ti6Al4V substrates did not, however, reveal inorganic nodules confirming that this was a HA-film-specific

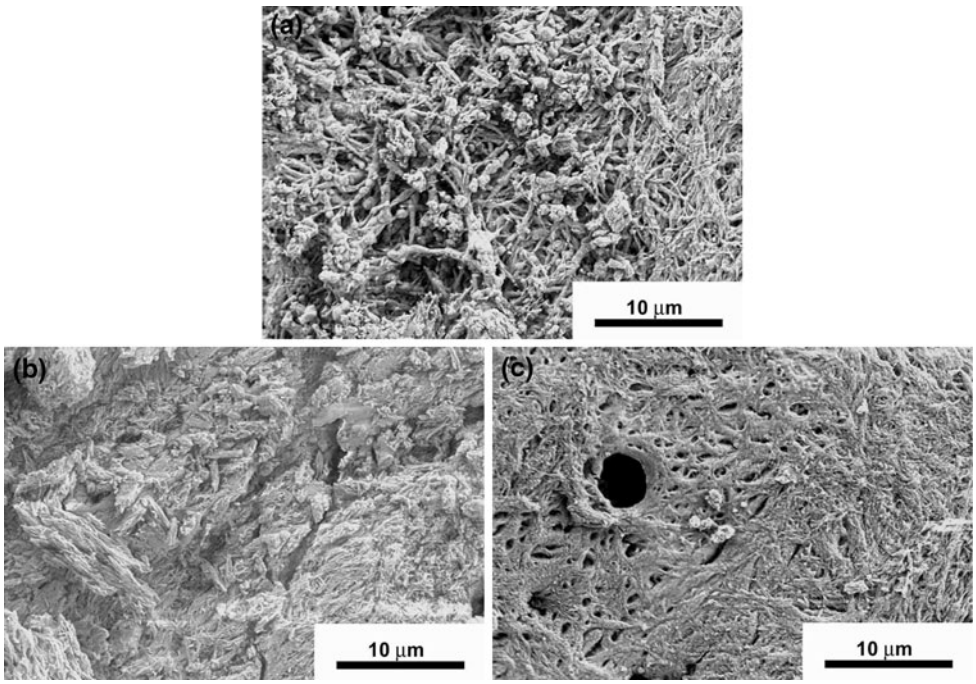

Fig. 5 Scanning electron micrographs of biomineral harvested from various substrates seeded with MC3T3-E1 subclone 4 p.15 osteoblast-like cells after 98 days in culture: **a** TCP, **b** P-Ti6Al4V, **c** R-Ti6Al4V

phenomenon (data not shown). This nodular inorganic phase is similar to biomineralized HA deposited in vitro and in vivo on HA films observed by others [36–39]. The nodules do not appear to have a preferential epitaxial relationship with the two populations of crystallographic faces provided by the film. Nodules appear to be adhered to both $\{10\bar{1}0\}$ (6 equivalent hexagonal faces) and $\{0001\}$ (2 equivalent faces that cap the hexagonal rod) crystallographic faces. It is concluded then that 10, 14, and 24 h HA films support the differentiation of MC3T3-E1 pre-osteoblast into fully differentiated, mineralizing osteoblasts. Because the deposited mineral is associated with the HA film and cannot be removed by chemical means, it may also be concluded that there is a direct chemical bond between the HA film and the biomineral. Interestingly, other HA films that are reported to be biomineral bonding have not necessarily had the biomineral-HA film bond challenged by chemical attack [37–39]. Thus, these

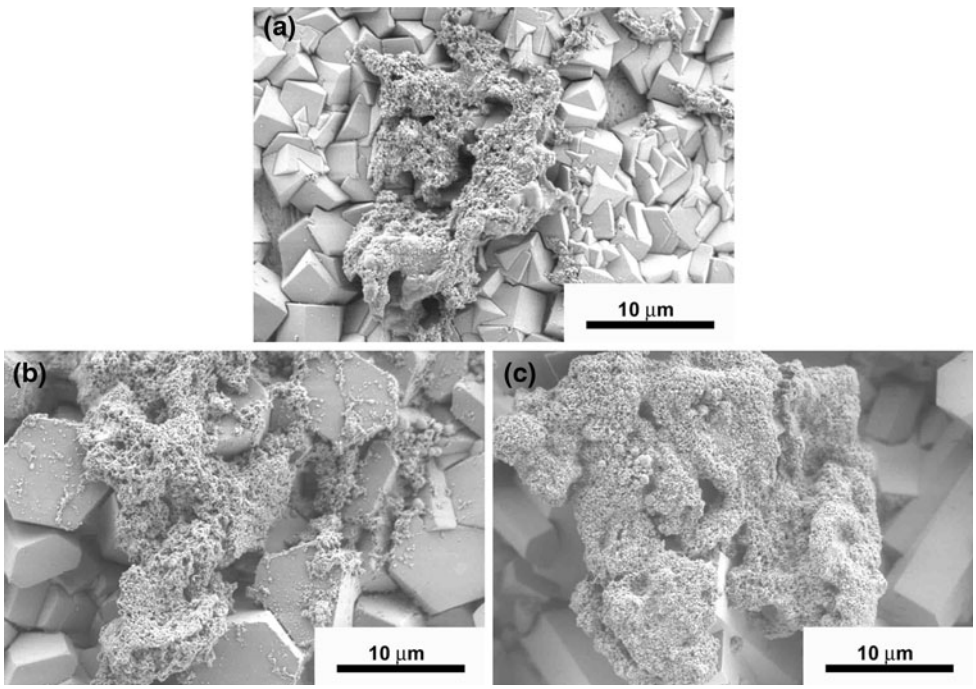

Fig. 6 Scanning electron micrographs of biomineral on the surface of various substrates seeded with MC3T3-E1 subclone 4 p.15 osteoblast-like cells after 98 days in culture: **a** HA 10 h, **b** HA 14 h, **c** HA 24 h

hydrothermally synthesized HA films are concluded to be biomineral bonding and osteoconductive in addition to bioactive.

4 Discussion

In a previous study, SEM analysis of the internal angles between adjacent equivalent faces of hexagonal grains and the application of Steno's Law demonstrated that the films reported here were composed of hexagonal single crystals of HA [22]. Importantly, molecular modeling and in vitro studies have shown that a number of acidic bone proteins and other proteins found to bind HA with high affinity, bind to the $\{10\bar{1}0\}$ crystallographic face of HA, which is prominently displayed on the six equivalent faces of hexagonal single crystals [23, 24]. Previous results also demonstrated that these films are high crystallinity, Ca-P phase-pure, passivating, and chemically bonded to titanium substrates [21, 22]. Thus, it was hypothesized that the films reported here would demonstrate robust bioactivity due to the functionalization of the film surface with highly bioactive HA crystallographic faces, which together with material properties, including film-substrate chemical bonding, would make these films potential candidates for use on clinical orthopedic implants such as Ti6Al4V.

Analysis of MC3T3-E1 subclone 4 pre-osteoblast spreading, metabolic activity (Alamar Blue^{TM} assay), and differentiation confirmed this hypothesis. Hydrothermally synthesized HA films reported here were found to be non-toxic (confirmed by cell spreading), bioactive (confirmed by metabolic activity and differentiation/extracellular matrix results), osteoconductive (confirmed by cell differentiation/mineralization study), and biomineral bonding (confirmed by cell differentiation/mineralization study) at levels comparable to the highest performing HA films reported elsewhere [31, 33, 34, 36–39]. The biomineral bonding characteristic of these films is particularly interesting. In review of the literature, Ducheyne et al. reported that biomineral bonding is the combined result of physiochemical processes including dissolution, precipitation, and ion-exchange and protein adsorption and cellular processes, which occur as a result of physiochemical processes [40]. Davies et al. have reasoned, however, that independent cell-mediated formation of cement lines—a mineralized collagen free matrix that serves as an interface between new and old bone—together with physiochemical processes enabled biomineral bonding in a material dependent fashion [38]. Data from de Bruijin et al. [37] support this claim demonstrating mineralized glycosaminoglycan (GAG)-positive layers of increasing size and decreasing GAG density at the film–ECM interface of HA films with decreasing crystallinity. Epitaxial growth of biomineral on the HA film surface has also been cited as a potential biomineral bonding mechanism [36, 37]. The films reported in this study are highly crystalline (99%+) [21] and do not demonstrate surface pitting due to dissolution after 98 days in cell culture in SEM micrographs. Findings from preliminary, dissolution studies in protein free physiological solution confirm this result, reporting the release of only 0.17 ppm of Ca^{2+} (Atomic Absorption Spectroscopy, model 4000, Perkin Elmer, Waltham, MA) from the films and into solution and no surface pitting after 1 month. Therefore, dissolution and precipitation do not likely play a large role in biomineral bonding here. Biomineral bonding on these films then is likely due to one or a combination of cellular processes and epitaxy. Irrespective of bonding mechanism, the biological properties of these HA films in combination with previously described crystallinity, phase, adhesion, and passivation characteristics, suggest that these films are excellent candidates for use as coatings on Ti6Al4V orthopedic implants.

Previous work also demonstrated that the [0001], *c*-axis, crystallographic orientation (texture) of hexagonal single crystals of HA could be engineered through control of synthesis time [22]. By taking advantage of the ability to control the crystal surfaces (faces) presented to the extracellular medium through control of crystallographic texture, and based on $\{10\bar{1}0\}$ HA–protein adsorption studies cited above it was thought that this film deposition process might enable a novel route to further functionalize the film surface with bioactive crystallographic faces. More specifically, it was hypothesized that engineering the orientation of hexagonal HA crystals should, together with aspect ratio and crystal spacing, enable the ratio of $\{10\bar{1}0\}/\{0001\}$ faces presented to the extracellular fluid to be altered, allowing modulation of protein adsorption, bioactivity, and potentially properties such as implant integration and healing time (see Sect. 1 for more details).

Analysis of MC3T3-E1 subclone 4 pre-osteoblast spreading, metabolic activity (Alamar Blue^{TM} assay), and differentiation was not able to affirm the hypothesis above. These studies found no significant difference in bioactivity on films synthesized for 10 h that have a nominally random [0001] crystallographic orientation, for 24 h that have a [0001] orientation several multiples greater than expected for a randomly oriented sample at $2\theta = 0°$, or for 14 h that have an intermediate [0001] texture [22]. This finding may be due to a number of reasons. One potential explanation is that bioactivity, as measured in this study, may not be sensitive to the limited [0001] orientation differences of the 10, 14, and 24 h samples. If samples representing more limiting cases of [0001] orientation could be crystallized, such that all crystals were either oriented at $2\theta = 0°$ or $2\theta = 90°$ and only the $\{10\bar{1}0\}$ or the $\{0001\}$ faces were displayed to the extracellular fluid, a significant increase in

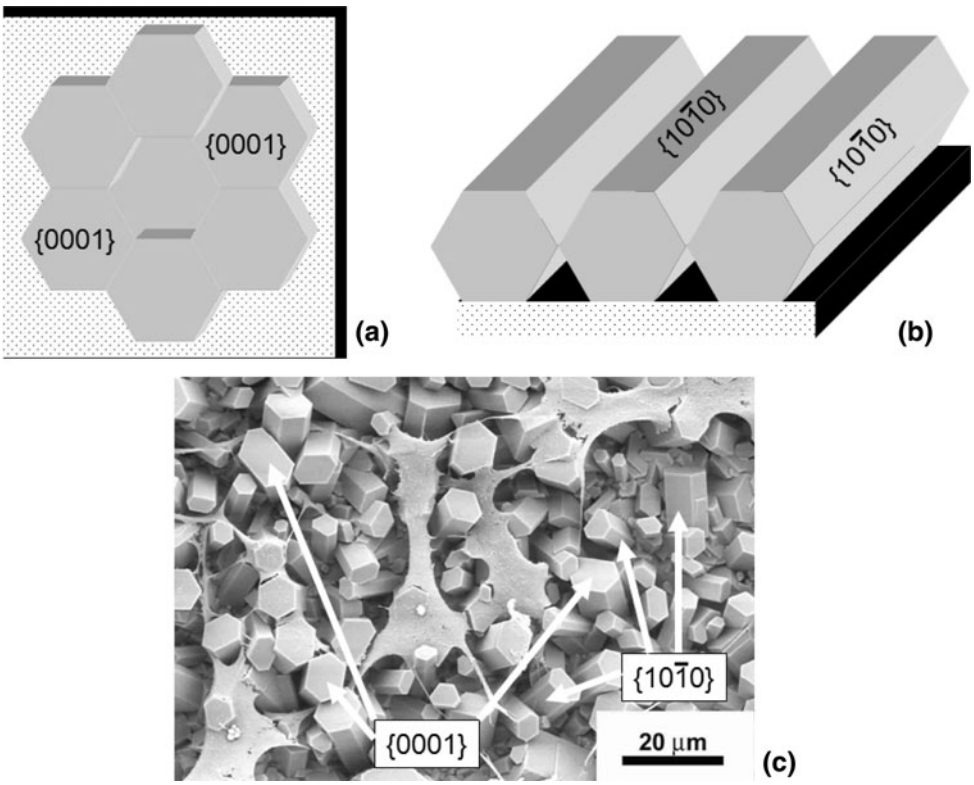

Fig. 7 Limiting cases of [0001] preferred orientation of HA films composed of hexagonal single crystals of HA. **a** A HA film composed of hexagonal single crystals with all crystals having a preferred [0001] orientation at $2\theta = 0°$ will only present {0001} crystallographic faces to the body. **b** A HA film composed of hexagonal single crystals with all crystals having a preferred [0001] orientation at $2\theta = 90°$ will only present $\{10\bar{1}0\}$ crystallographic faces to the body. **c** Indexed micrograph of HA film from Fig. 1e

bioactivity on the former sample might still be expected. Figure 7 graphically displays these limiting cases. It is also feasible that although care was taken to account for both surface roughness and [0001] crystallographic orientation, the effect of these variables masked each other. As evidence, Kim et al. has reported significant differences in cell proliferation between Ti surfaces that vary in surface roughness on the same scale as in the HA films reported here, ~1–3 μm. Thus, based on surface roughness alone, a significant decrease in total metabolic activity with increasing surface roughness and synthesis time should be expected across the HA films.

It is also feasible that reported differences in $\{10\bar{1}0\}$ and {0001} protein adsorption are incompletely understood. For example, Fujisawa et al. reports that a number of acidic bone proteins including phosphophoryn, osteocalcin (bone Gla protein), osteonectin, and bone small proteoglycan II are all preferentially adsorbed on the $\{10\bar{1}0\}$ equivalent plane in vitro [24]. However, Flade et al. [41] reports preferential adsorption of osteocalcin onto the {0001} equivalent plane in vitro. Thus, there are inconsistencies in the literature regarding which plane specific proteins preferentially adsorb to. One or a combination of three factors may explain differences in the results of Fujisawa et al. and Flade et al. The first factor is protein concentration. Fujisawa et al. utilized protein concentrations of 1–100 μg/ml for binding studies, while Flade et al. utilized a protein concentration of 250 μg/ml. Consequently, protein concentration differences of this magnitude have been demonstrated to affect protein–mineral interactions [42]. The second factor relates to the use of buffers. Fujisawa et al. utilized a trishydroxymethylaminomethane (Tris)–HCl/NaCl buffer, while Flade et al. utilized a Na_3PO_4/NaCl buffer at different salt concentrations. Consequently, changing concentrations of salts, especially phosphate salts, are known to modulate protein–HA adsorption [43]. The third factor is the hydroxyapatite used for the binding experiments. Both manuscripts made a qualitative assessment of the HA crystal faces presented to the protein solutions in their experiments based on HA grain morphology. Neither manuscript explicitly characterizes the crystallography of the HA that is used for adsorption experiments. This is in contrast to the films reported in this study, which previously underwent a careful and detailed analysis including pole figure orientation analysis to determine the crystal faces presented to the extracellular fluid [22]. Consequently, the omission of a robust analysis of the crystallography of the HA utilized in each study confounds the resulting conclusions reached by Fujisawa et al. and Flade et al. Thus, it seems that more comprehensive and robust studies of the interaction of individual bone proteins in physiological solution with well-characterized HA crystals need to be undertaken.

Even if more comprehensive and robust studies of the interaction of individual bone proteins in physiological solution with specific HA crystal faces are undertaken,

their applicability to the cellular or tissue scale bioactivity of implanted HA is unclear given the results of this manuscript. First, competitive protein adsorption from serum, which contains numerous proteins is a different and much more complex process than single protein adsorption experiments. HA is well known to bind numerous proteins regardless of specific crystallographic faces, which is why HA is used as a substrate in protein chromatography. Under physiological conditions, a single protein will adsorb onto the surface of HA in the presence of numerous other serum proteins and bio-molecules after implantation. This competitive adsorption means that the proteins that adsorb to HA non-specifically may inhibit or severely limit the crystallographic face specific protein adsorption observed in single protein experiments. At the tissue level, the cell-mediated formation of cement lines at HA implant interfaces noted above may further make HA crystallographic face specific protein adsorption a moot point. Thus, while crystallographic face specific protein adsorption experiments may help model and explain phenomenon such as the nucleation and growth of individual mineral crystals, it may not be applicable to phenomenon such as bulk implant bioactivity given the results of this manuscript.

5 Conclusions

The high crystallinity, Ca-P phase-pure, adhesive, passivating, HA films deposited by TEP/EDTA doubly regulated hydrothermal crystallization on Ti6Al4V substrates examined in this study were found to be non-toxic, biocompatible, bioactive, osteoconductive, and biomineral bonding. Differences in the [0001] crystallographic orientation of the hexagonal HA single crystals, which compose the film, were not found to cause a significant difference in these parameters. The lack of significant bioactivity differences indicates that there may be no relationship between HA crystallographic face specific protein adsorption and bulk HA bioactivity. Nonetheless, based on material and biological properties it is concluded that these films should be considered as candidates for use on clinical Ti6Al4V orthopedic implants.

Acknowledgements We gratefully acknowledge support from the Rutgers Center for Ceramic Research, the National Science Foundation/Rutgers IGERT on Biointerfaces, which supported both D.J. Haders and C.C. Kazanecki, the Department of Education/Rutgers GAANN in Molecular, Cellular, and Nanosystems Bioengineering, the Rutgers University Graduate School New Brunswick, the New Jersey Center for Biomaterials, the Rutgers University Roger G. Ackerman Fellowship, and the Rutgers University Technology Commercialization Fund. The authors would like to thank Alexander Burukhin for his contribution to this work as well as Valentin Starovoytov for sputter coating biological specimens.

References

1. Cheang P, Khor KA. Addressing processing problems associated with plasma spraying of hydroxyapatite coatings. Biomaterials. 1996;17(5):537–44.
2. Tsui YC, Doyle C, Clyne TW. Plasma sprayed hydroxyapatite coatings on titanium substrates. Part 1: mechanical properties and residual stress levels. Biomaterials. 1998;19(22):2015–29.
3. Sun L, et al. Material fundamentals and clinical performance of plasma-sprayed hydroxyapatite coatings: a review. J Biomed Mater Res. 2001;58(5):570–92.
4. Porter AE, et al. Bone bonding to hydroxyapatite and titanium surfaces on femoral stems retrieved from human subjects at autopsy. Biomaterials. 2004;25(21):5199–208.
5. Browne M, Gregson PJ. Effect of mechanical surface pretreatment on metal ion release. Biomaterials. 2000;21(4):385–92.
6. Park E, et al. Interfacial characterization of plasma-spray coated calcium phosphate on Ti–6Al–4V. J Mater Sci Mater Med. 1998;9(11):643–9.
7. Filiaggi MJ, Coombs NA, Pilliar RM. Characterization of the interface in the plasma-sprayed HA coating/Ti–6Al–4V implant system. J Biomed Mater Res. 1991;25(10):1211–29.
8. Ji H, Ponton CB, Marquis PM. Microstructural characterization of hydroxyapatite coating on titanium. J Mater Sci Mater Med. 1992;3:283–7.
9. Geesink RG. Osteoconductive coatings for total joint arthroplasty. Clin Orthop Relat Res. 2002;(395):53–65.
10. LeGeros RZ, Craig RG. Strategies to affect bone remodeling: osteointegration. J Bone Miner Res. 1993;8(Suppl 2):S583–96.
11. Spivak JM, et al. A new canine model to evaluate the biological response of intramedullary bone to implant materials and surfaces. J Biomed Mater Res. 1990;24(9):1121–49.
12. Kangasniemi IM, et al. In vivo tensile testing of fluorapatite and hydroxylapatite plasma-sprayed coatings. J Biomed Mater Res. 1994;28(5):563–72.
13. Lin H, et al. Tensile tests of interface between bone and plasma-sprayed HA coating-titanium implant. J Biomed Mater Res. 1998;43(2):113–22.
14. Dalton JE, Cook SD. In vivo mechanical and histological characteristics of HA-coated implants vary with coating vendor. J Biomed Mater Res. 1995;29(2):239–45.
15. Suchanek W, Yoshimura M. Processing and properties of hydroxyapatite-based biomaterials for use as hard tissue replacement implants. J Mater Res. 1998;13(1):94–117.
16. Wang D, et al. Effects of sol–gel processing parameters on the phases and microstructures of HA films. Colloids Surf B Biointerfaces. 2007;57(2):237–42.
17. van Dijk K, et al. Influence of annealing temperature on RF magnetron sputtered calcium phosphate coatings. Biomaterials. 1996;17(4):405–10.
18. Ong JL, Lucas LC. Post-deposition heat treatments for ion beam sputter deposited calcium phosphate coatings. Biomaterials. 1994;15(5):337–41.
19. Jonasova L, et al. Biomimetic apatite formation on chemically treated titanium. Biomaterials. 2004;25(7–8):1187–94.
20. Garcia F, et al. Effect of heat treatment on pulsed laser deposited amorphous calcium phosphate coatings. J Biomed Mater Res. 1998;43(1):69–76.
21. Haders D, et al. TEP/EDTA doubly regulated hydrothermal crystallization of hydroxyapatite on metal substrates. Chem Mater. 2008;20(22):7177–87.
22. Haders DJ, et al. Phase sequenced deposition of calcium titanate/hydroxyapatite films with controllable crystallographic texture onto Ti6Al4V by TEP regulated hydrothermal crystallization. Crystal Growth Des. 2009;9(8):3412–22.

23. Huq NL, Cross KJ, Reynolds EC. Molecular modeling of a mutiphosphorylated sequence motif bound to hydroxyapatite surfaces. J Mol Model. 2000;6:35–47.
24. Fujisawa R, Kuboki Y. Preferential adsorption of dentin and bone acidic proteins on the (100) face of hydroxyapatite crystals. Biochim Biophys Acta. 1991;1075(1):56–60.
25. Sawyer AA, Hennessy KM, Bellis SL. The effect of adsorbed serum proteins, RGD and proteoglycan-binding peptides on the adhesion of mesenchymal stem cells to hydroxyapatite. Biomaterials. 2007;28(3):383–92.
26. Linez-Bataillon P, et al. In vitro MC3T3 osteoblast adhesion with respect to surface roughness of Ti6Al4V substrates. Biomol Eng. 2002;19(2–6):133–41.
27. Kim MJ, et al. Microrough titanium surface affects biologic response in MG63 osteoblast-like cells. J Biomed Mater Res A. 2006;79(4):1023–32.
28. Green JR, Margerison D. Statistical treatment of experimental data. New York: Elsevier Scientific Publishing Company; 1978. p. 382.
29. Wang D, et al. Isolation and characterization of MC3T3–E1 preosteoblast subclones with distinct in vitro and in vivo differentiation/mineralization potential. J Bone Miner Res. 1999;14(6):893–903.
30. Franceschi RT, Iyer BS. Relationship between collagen synthesis and expression of the osteoblast phenotype in MC3T3-E1 cells. J Bone Miner Res. 1992;7(2):235–46.
31. Chou YF, et al. The effect of biomimetic apatite structure on osteoblast viability, proliferation, and gene expression. Biomaterials. 2005;26(3):285–95.
32. Soboyejo WO, et al. Interactions between MC3T3-E1 cells and textured Ti6Al4V surfaces. J Biomed Mater Res. 2002;62(1):56–72.
33. Ball MD, et al. Osteoblast growth on titanium foils coated with hydroxyapatite by pulsed laser ablation. Biomaterials. 2001;22(4):337–47.
34. Thian ES, et al. Magnetron co-sputtered silicon-containing hydroxyapatite thin films—an in vitro study. Biomaterials. 2005;26(16):2947–56.
35. Ohgushi H, et al. In vitro bone formation by rat marrow cell culture. J Biomed Mater Res. 1996;32(3):333–40.
36. Bagambisa FB, Joos U, Schilli W. Mechanisms and structure of the bond between bone and hydroxyapatite ceramics. J Biomed Mater Res. 1993;27(8):1047–55.
37. de Bruijin JD, et al. Analysis of the bony interface with various types of hydroxyapatite in vitro. Cells Mater. 1993;3(2):115–27.
38. Davies JE, Baldan N. Scanning electron microscopy of the bone-bioactive implant interface. J Biomed Mater Res. 1997;36(4):429–40.
39. de Bruijn JD, Bovell YP, van Blitterswijk CA. Structural arrangements at the interface between plasma sprayed calcium phosphates and bone. Biomaterials. 1994;15(7):543–50.
40. Ducheyne P, Qiu Q. Bioactive ceramics: the effect of surface reactivity on bone formation and bone cell function. Biomaterials. 1999;20(23–24):2287–303.
41. Flade K, et al. Osteocalcin-controlled dissolution-reprecipitation of calcium phosphate under biomimetic conditions. Chem Mater. 2001;13:3596–602.
42. Boskey AL, et al. Concentration-dependent effects of dentin phosphophoryn in the regulation of in vitro hydroxyapatite formation and growth. Bone Miner. 1990;11(1):55–65.
43. Schmidt SR, Schweikart F, Andersson ME. Current methods for phosphoprotein isolation and enrichment. J Chromatogr B Anal Technol Biomed Life Sci. 2007;849(1–2):154–62.